




BRIEF DEFINITIVE REPORT

Irg1 expression in myeloid cells prevents immunopathology during *M. tuberculosis* infection

Sharmila Nair^{1*}, Jeremy P. Huynh^{2*}, Vicky Lampropoulou³, Ekaterina Loginicheva³, Ekaterina Esaulova^{3,4} , Anshu P. Gounder², Adrianus C.M. Boon^{1,2,3} , Elizabeth A. Schwarzkopf³, Tara R. Bradstreet³, Brian T. Edelson³, Maxim N. Artyomov³, Christina L. Stallings², and Michael S. Diamond^{1,2,3,5} 

Immune-Responsive Gene 1 (Irg1) is a mitochondrial enzyme that produces itaconate under inflammatory conditions, principally in cells of myeloid lineage. Cell culture studies suggest that itaconate regulates inflammation through its inhibitory effects on cytokine and reactive oxygen species production. To evaluate the functions of Irg1 in vivo, we challenged wild-type (WT) and *Irg1*^{-/-} mice with *Mycobacterium tuberculosis* (*Mtb*) and monitored disease progression. *Irg1*^{-/-}, but not WT, mice succumbed rapidly to *Mtb*, and mortality was associated with increased infection, inflammation, and pathology. Infection of *LysM*-Cre *Irg1*^{fl/fl}, *Mrp8*-Cre *Irg1*^{fl/fl}, and *CD11c*-Cre *Irg1*^{fl/fl} conditional knockout mice along with neutrophil depletion experiments revealed a role for Irg1 in *LysM*⁺ myeloid cells in preventing neutrophil-mediated immunopathology and disease. RNA sequencing analyses suggest that Irg1 and its production of itaconate temper *Mtb*-induced inflammatory responses in myeloid cells at the transcriptional level. Thus, an Irg1 regulatory axis modulates inflammation to curtail *Mtb*-induced lung disease.

Introduction

Mycobacterium tuberculosis (*Mtb*), the etiologic agent of tuberculosis (TB), causes up to 8.8 million new clinical infections and 1.4 million deaths annually (World Health Organization, 2016). In the mouse model of TB, the acute phase of infection is marked by exponential growth of the bacteria in the lungs. In its persistence phase, *Mtb* undergoes a metabolic shift, triggered by changes in nutrient availability as substrates for glycolysis become limited (Bloch and Segal, 1956). The bacterial glyoxylate shunt pathway is an alternative anaplerotic pathway that facilitates the use of fatty acids as a carbon source for biosynthetic pathways and generation of ATP. *Mtb* strains encode at least one and sometimes two isocitrate lyases (ICL1 and ICL2) that function within the glyoxylate shunt (Höner Zu Bentrup et al., 1999; Dunn et al., 2009). Mutation of the ICL genes has provided evidence for a role of the glyoxylate shunt in *Mtb* pathogenesis (McKinney et al., 2000; Muñoz-Elías and McKinney, 2005).

The host Immune-Responsive Gene 1 (*Irg1*; also called *Acod1*) is a mitochondrial enzyme induced under inflammatory conditions that produces the metabolite itaconate by decarboxylating cis-aconitate, a TCA cycle intermediate (Michelucci et al.,

2013). Because itaconate production in myeloid cells reportedly inhibits bacterial ICLs, it has gained interest as an endogenous antibacterial effector molecule (McFadden and Purohit, 1977). This role was supported by a study showing that nonphysiologically relevant (25 mM) concentrations of itaconate had bacteriostatic effects on *Mtb* growth during liquid culture under conditions requiring the glyoxylate shunt pathway (Michelucci et al., 2013).

Beyond its possible antibacterial functions, itaconate also links immune cell metabolism and inflammatory responses. *Irg1* is highly expressed in macrophages in response to proinflammatory stimuli that induce type I and type II IFN signaling (Degrandi et al., 2009). In bone marrow-derived macrophages (BMDMs), itaconate suppressed the production of mitochondrial ROS as well as proinflammatory cytokines, including IL1-β, IL6, and IL12p70 (Lampropoulou et al., 2016). This capacity to modulate inflammation could be of particular importance during *Mtb* infection because excessive immune responses can prevent bacterial clearance and cause pathology (Nandi and Behar, 2011; Kimmey et al., 2015).

¹Department of Medicine, Washington University School of Medicine, St. Louis, MO; ²Department of Molecular Microbiology, Washington University School of Medicine, St. Louis, MO; ³Department of Pathology & Immunology, Washington University School of Medicine, St. Louis, MO; ⁴Computer Technologies Department, ITMO University, Saint Petersburg, Russia; ⁵The Andrew M. and Jane M. Bursky Center for Human Immunology and Immunotherapy Programs, Washington University School of Medicine, St. Louis, MO.

*S. Nair and J.P. Huynh contributed equally to this paper; Correspondence to Michael S. Diamond: diamond@wustl.edu; Christina L. Stallings: stallings@wustl.edu.

© 2018 Nair et al. This article is distributed under the terms of an Attribution–Noncommercial–Share Alike–No Mirror Sites license for the first six months after the publication date (see <http://www.rupress.org/terms/>). After six months it is available under a Creative Commons License (Attribution–Noncommercial–Share Alike 4.0 International license, as described at <https://creativecommons.org/licenses/by-nc-sa/4.0/>).

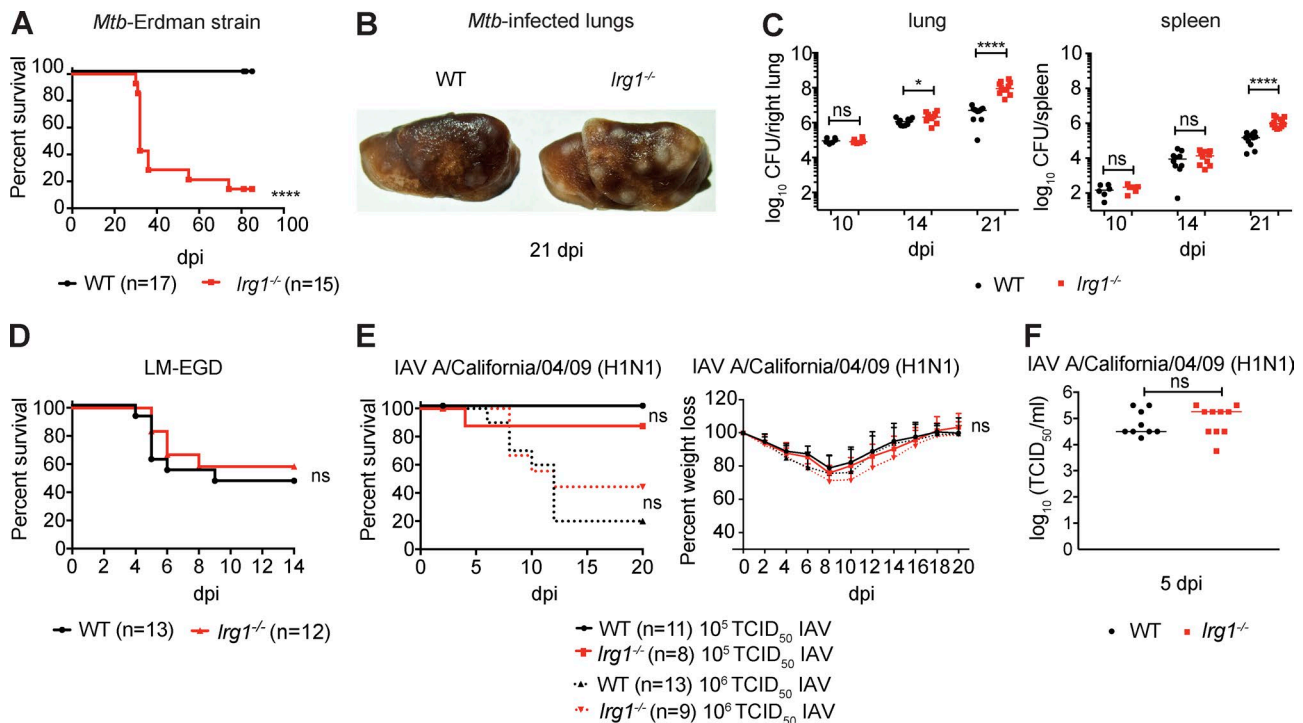


Figure 1. Irg1 is essential for host resistance to *Mtb*. (A–C) WT and *Irg1*^{-/-} mice were infected with aerosolized *Mtb*. (A) Survival analysis. (B) Gross pathology of lungs at day 21. (C) *Mtb* burden (GFP⁺ Erdman strain) was measured at days 10 (*n* = 6), 14 (*n* = 10), and 21 (*n* = 11–12) after infection. (D) WT and *Irg1*^{-/-} mice were inoculated intravenously with *Listeria monocytogenes* (LM) and monitored for survival (*n* = 12–13). (E and F) WT and *Irg1*^{-/-} mice were infected intranasally with IAV and monitored for survival and weight loss (E), and lung viral burden at 5 dpi (F; *n* = 9–10). (A–F) All data are from at least two independent experiments. Statistical differences are indicated. (C, E [right], and F) Mann-Whitney test: *, *P* < 0.05; ****, *P* < 0.0001; ns, not significant. (A, D, and E [left]) Log-rank test. ns, not significant. Error bars designate SEM.

We addressed the function of *Irg1* in regulating immune responses and *Mtb* pathogenesis using *Irg1*^{-/-} and *Irg1*^{fl/fl} conditional gene-deleted mice. A complete absence of *Irg1* during *Mtb* infection resulted in severe pulmonary disease and ultimately death, with greater numbers of infected myeloid cells and higher production of inflammatory cytokines and chemokines. *Irg1* expression in myeloid cell subsets was necessary to control neutrophil recruitment, *Mtb* infection, and immune-mediated tissue injury. Our studies define a key role for *Irg1* in regulating immune cell metabolism in subsets of myeloid cells, which minimizes the pathological immune response that contributes to pulmonary disease caused by *Mtb*.

Results and discussion

To determine the role of *Irg1* during *Mtb* infection, *Irg1*^{-/-} C57BL/6N mice were monitored for clinical and bacterial outcomes after aerosol inoculation with the *Mtb* Erdman strain. Whereas all WT mice survived past 80 d postinfection (dpi), ~75% of *Irg1*^{-/-} mice succumbed to *Mtb* within 30 d, a phenotype similar to animals lacking IFN- γ signaling (Fig. 1 A; Cooper et al., 1993; Flynn et al., 1993; Nandi and Behar, 2011). At 21 dpi, the lungs of *Irg1*^{-/-} mice infected with *Mtb* had larger numbers and sizes of macroscopic lesions compared with infected WT mice (Fig. 1 B). Although bacterial levels were similar in the lungs and spleens of WT and *Irg1*^{-/-} mice at 10 dpi, by 14 and 21 dpi, the *Mtb* burden was ~3- and 25-fold higher, respectively, in the lungs

of *Irg1*^{-/-} compared with WT mice (*P* < 0.01; Fig. 1 C, left). At 21 dpi, *Mtb* burden also was approximately eightfold higher in the spleens of *Irg1*^{-/-} compared with WT mice (Fig. 1 C, right). We also tested the effects of *Irg1* on *Listeria monocytogenes* (strain EGD), an intracellular bacterium administered by intravenous injection, and Influenza A virus (IAV strain A/California/04/2009 H1N1), a respiratory pathogen inoculated by intranasal route (Fig. 1, D–F). Loss of *Irg1* expression in mice did not result in altered susceptibility to *Listeria monocytogenes* (Fig. 1 D) or IAV infection (Fig. 1, E and F).

The strain of *Mtb* used in this study, Erdman, encodes two ICL genes, *ICL1* and *ICL2*. In vivo, Δ *icl1* *Mtb* strains replicate normally during the acute phase, but are attenuated during the chronic, persistent phase of infection, whereas Δ *icl2* *Mtb* strains show no defects in infection (McKinney et al., 2000; Muñoz-Eliás and McKinney, 2005). Δ *icl1* Δ *icl2* strains are avirulent in vivo, possibly because ICL has additional methylsuccinate lyase activity that prevents toxic accumulation of propionyl-CoA (Muñoz-Eliás and McKinney, 2005; Muñoz-Eliás et al., 2006; Savvi et al., 2008). To test the impact of *Irg1* on the bacterial glyoxylate shunt in vivo, we infected WT and *Irg1*^{-/-} mice with WT and isogenic Δ *icl1* *Mtb* strains. As anticipated, 100% of WT mice infected with WT or Δ *icl1* *Mtb* survived infection over an 80-d time course (Fig. S1 A). In contrast, all *Irg1*^{-/-} mice infected with Δ *icl1* *Mtb* succumbed to infection without differences in mean time to death (Fig. S1 A) or relative weight loss (Fig. S1 B) compared with the isogenic WT *Mtb* strain. Moreover, Δ *icl1* bacterial titers in the lung and

the spleen of *Irg1*^{-/-} mice were ~83- and ~12-fold higher than in WT mice, respectively (Fig. S1 C). Because *Δicl1 Mtb* lacks a fully functional glyoxylate shunt pathway, yet is still virulent in *Irg1*^{-/-} mice, *Irg1* likely restricts *Mtb* infection in vivo independently of its activity on ICL1.

We next evaluated whether *Irg1*-dependent regulation of inflammatory responses (Lampropoulou et al., 2016) contributed to *Mtb* pathogenesis. We infected WT and *Irg1*^{-/-} mice with an *Mtb* strain expressing GFP (*Mtb*-GFP) that has the same virulence properties as WT *Mtb* (Fig. S1 F). Histological analysis at 21 dpi showed that lung lesions from *Mtb*-GFP-infected *Irg1*^{-/-} mice were larger in size with denser cellular infiltrates (Fig. 2 A). To define the composition of these infiltrates, we profiled immune cells in *Mtb*-GFP-infected lungs by flow cytometry (gating strategy defined in Fig. S2 A). At 10 dpi, no differences in the number of neutrophils, inflammatory monocytes, infiltrating macrophages, alveolar macrophages, dendritic cells, natural killer (NK) and NKT cells, or eosinophils were detected in the lungs of WT and *Irg1*^{-/-} mice (Fig. 2, B and C). However, by day 14, infected lungs from *Irg1*^{-/-} mice had greater numbers of neutrophils (approximately fourfold) and eosinophils (threefold) than WT mice, and this difference remained at day 21 for neutrophils (Fig. 2, B, D, and E). At 21 dpi, lungs from *Irg1*^{-/-} mice also had lower numbers of alveolar macrophages (1.3-fold) and NK1.1⁺ cells (approximately threefold). Analysis of other innate immune cell populations in the lungs at 14 and 21 dpi revealed no significant differences in numbers of inflammatory monocytes, infiltrating macrophages, and infiltrating and resident dendritic cells between *Mtb*-GFP-infected WT and *Irg1*^{-/-} mice. In addition, no differences in the numbers of CD4⁺ T cells, CD8⁺ T cells, and B cells were found between WT and *Irg1*^{-/-} mice at 21 dpi (Fig. S2 B).

We measured the effect of *Irg1* on the accumulation of inflammatory mediators in the lung during *Mtb*-GFP infection. Equivalent levels of chemokines and proinflammatory cytokines in lung homogenates of WT and *Irg1*^{-/-} mice were detected at 10 dpi (Fig. 2 F and Fig. S2 C). By 14 dpi, higher levels of several proinflammatory cytokines (IL1-β, IL6, IL17, and G-CSF) and chemokines (CXCL1, CCL3, and CCL4) were detected in the lungs of *Irg1*^{-/-} mice compared with WT mice (Fig. 2 G), although TNF-α levels remained unchanged (Fig. S2 C). By 21 dpi, all proinflammatory cytokines (IL1-β, IL6, IL12p70, IL17, IFN-γ, TNF-α, and G-CSF) and chemokines (CCL2, CXCL1, CCL3, and CCL4) measured were higher in the lungs of *Irg1*^{-/-} mice compared with WT mice (Fig. 2 H and Fig. S2 C).

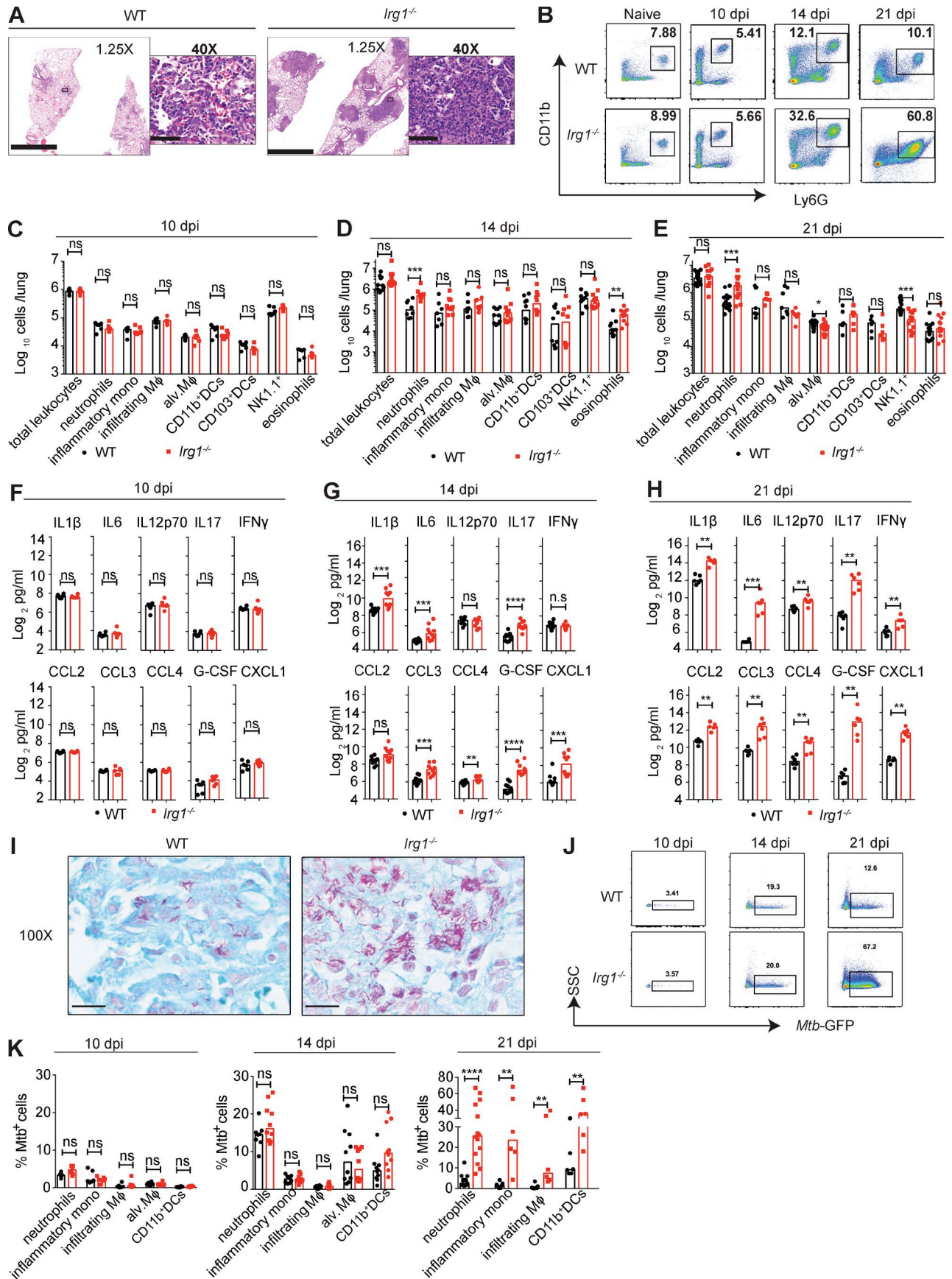
Because *Irg1*^{-/-} mice infected with WT or *Δicl1 Mtb* succumbed to infection at equivalent rates (Fig. S1 A), we investigated if the inflammatory responses in these mice was similar. *Δicl1 Mtb*-infected *Irg1*^{-/-} mice also showed increased accumulation of neutrophils in their lungs at 21 dpi (Fig. S1 D). Correspondingly, proinflammatory cytokines (IL1-β, IL6, IL12p70, IL17, G-CSF, and IFN-γ) and chemokines (CCL2, CCL3, CCL4, and CXCL1) were higher in *Δicl1 Mtb*-infected *Irg1*^{-/-} mice compared with WT mice (Fig. S1 E). The similar levels of increased neutrophil accumulation in response to both WT and *Δicl1 Mtb* in *Irg1*^{-/-} mice supports the hypothesis that the defect in controlling *Mtb* infection in these mice is independent of ICL1 activity and a fully functional glyoxylate shunt pathway.

We evaluated whether accumulating myeloid cells in the lung were infected with *Mtb*. At 21 dpi, lung lesions were the preferred sites for *Mtb* infection, with greater numbers of acid-fast bacilli present in *Irg1*^{-/-} mice (Fig. 2 I). To analyze infection in each myeloid cell type, we monitored the presence of *Mtb*-GFP by flow cytometry. At 10 and 14 dpi, each myeloid cell type in WT and *Irg1*^{-/-} lungs was infected at similar frequencies (Fig. 2, J and K). By 21 dpi, lungs from *Irg1*^{-/-} mice had higher percentages of infected neutrophils (eightfold), inflammatory monocytes (19-fold), infiltrating macrophages (19-fold), and CD11b⁺ dendritic cells (approximately threefold) compared with WT mice (Fig. 2, J and K). Collectively, this data suggests that *Irg1* regulates inflammatory responses, which controls the recruitment of multiple types of myeloid cells, many of which become targets for subsequent rounds of *Mtb* infection. *Irg1* did not have a direct effect on *Mtb* infectivity in cell culture, as no differences in bacterial titers were detected in WT and *Irg1*^{-/-} BMDMs (Fig. S1 G).

In macrophage-lineage cells from zebrafish, *Irg1* was suggested to promote antibacterial effects by regulating the use of fatty acids, which are substrates for mitochondrial ROS (mROS) production (Hall et al., 2013). To determine whether *Irg1*^{-/-} mice had less mROS expression in key myeloid cells as an explanation for the failure to control *Mtb* infection, we evaluated mROS levels in neutrophils in vivo at 21 dpi. However, neutrophils from *Mtb*-infected *Irg1*^{-/-} mice had a higher expression of mROS (Fig. S2 D). Exogenous itaconate treatment of activated BMDMs in vitro also was shown to suppress mROS and inducible nitric oxide synthase (iNOS) expression (Lampropoulou et al., 2016). Consistent with these findings, *Irg1*^{-/-} mice had a higher frequency and number of iNOS-producing neutrophils (Fig. S2 D). Thus, the higher production of mROS and iNOS in *Irg1*^{-/-} neutrophils suggests these cells are in a hyperinflamed state, rather than being defective in these antimicrobial mediators.

To begin to define which cell types required *Irg1* expression to control *Mtb* infection, we established reciprocal bone marrow chimeric mice by replacing the WT and *Irg1*^{-/-} recipient marrow with the donor marrow cells from *Irg1*^{-/-} and WT mice or using WT marrow into donor WT mice as controls (Fig. S3 A). Whereas WT → WT and WT → *Irg1*^{-/-} mice survived *Mtb* infection for over 80 dpi, *Irg1*^{-/-} → WT mice succumbed to *Mtb* infection by 32 dpi, demonstrating that the protective response was derived from *Irg1*-sufficient radiosensitive cells (Fig. S3 B). *Mtb* titers in the lungs and the spleen of *Irg1*^{-/-} → WT mice were higher than WT → WT mice at 21 dpi (~10-fold and threefold, respectively; Fig. S3 C). At 21 dpi *Irg1*^{-/-} → WT mice had greater accumulation of neutrophils in their lungs than WT → WT mice (Fig. S3 D), whereas no differences in recruitment of other innate immune populations were seen.

Excessive neutrophil recruitment is associated with progression of *Mtb* disease (Nandi and Behar, 2011; Kimmey et al., 2015). To test whether the susceptibility of the *Irg1*^{-/-} mice to *Mtb* infection was a result of the increased accumulation of neutrophils in the lung, we administered a neutrophil-depleting (anti-Ly6G) or isotype control antibody to WT and *Irg1*^{-/-} mice, beginning on day 10 with repeated injections every other day through day 34. Treatment of *Irg1*^{-/-} mice from day 10 to 34 with anti-Ly6G prolonged survival during *Mtb* infection (Fig. 3 A). Depletion



of neutrophils starting at day 10 also resulted in reduced *Mtb* burden in the lungs at 21 dpi (19-fold) compared with isotype control-treated *Irg1*^{-/-} mice. However, the levels of *Mtb* in neutrophil-depleted *Irg1*^{-/-} mice still were higher (ninefold) than in antibody-treated WT mice (Fig. 3 B), indicating that recruitment and infection of neutrophils partially contributed to the higher bacterial burden in *Mtb*-infected *Irg1*^{-/-} mice. Correspondingly, diminished numbers of bacilli were present in lung sections of *Irg1*^{-/-} mice treated with anti-Ly6G mAb compared with the isotype control (Fig. 3 C). Lung lesions from *Mtb*-infected, anti-Ly6G mAb-treated *Irg1*^{-/-} mice were smaller than isotype-treated counterparts (Fig. 3 C). Cytokine and chemokine levels in the lung also were decreased in neutrophil-depleted *Irg1*^{-/-} mice at 21 dpi (Fig. 3 D). At 21 dpi, as expected, anti-Ly6G mAb treatment of *Irg1*^{-/-} mice had reduced the number of neutrophils compared with isotype control-treated animals (Fig. 3 E and Fig. S2 E). With the exception of a small decrease in numbers of inflammatory monocytes, the recruitment of which could be altered by decreases in lung cytokine and chemokine expression as a result of neutrophil depletion, all other innate immune cell subsets were unaffected by neutrophil depletion (Fig. 3 E). Once the neutrophil depletion treatment was stopped and neutrophils were allowed to accumulate in the lung, disease ensued and all *Irg1*^{-/-} mice succumbed to infection. Thus, depletion of neutrophils mitigates the bacterial and proinflammatory pathological phenotypes observed at day 21 after infection in *Irg1*^{-/-} mice, and a dysfunctional neutrophil response contributes to the susceptibility of these mice to *Mtb* infection.

We next sought to identify the cell types that expressed *Irg1* and modulated neutrophil accumulation and *Mtb* disease pathogenesis. Because *Irg1* is expressed principally in cells of myeloid lineage (Degrandi et al., 2009; Hall et al., 2013; Michelucci et al., 2013; Lampropoulou et al., 2016), we tested its role in *Mtb* infection in different myeloid cell subsets using mice lacking *Irg1* expression in neutrophils (*Mrp8*-Cre⁺ *Irg1*^{fl/fl}), alveolar macrophages and some dendritic cells (*CD11c*-Cre⁺ *Irg1*^{fl/fl}), or monocytes/macrophages, alveolar macrophages, neutrophils, and some dendritic cells (*LysM*-Cre⁺ *Irg1*^{fl/fl}; Fig. S3, E–G). Although all Cre⁻ *Irg1*^{fl/fl} and *Mrp8*-Cre⁺ *Irg1*^{fl/fl} mice survived past 150 dpi, all *LysM*-Cre⁺ *Irg1*^{fl/fl} mice succumbed to *Mtb* within 40 dpi, a phenotype similar to *Irg1*^{-/-} mice (Fig. 4 A). In comparison, all *CD11c*-Cre⁺ *Irg1*^{fl/fl} mice succumbed to *Mtb* by 135 dpi. Consistent with these survival results, *Mtb* levels in the lungs of *Mrp8*-Cre⁺ *Irg1*^{fl/fl} mice were similar to littermate Cre⁻ *Irg1*^{fl/fl} controls, whereas *CD11c*-Cre⁺ *Irg1*^{fl/fl} and *LysM*-Cre⁺ *Irg1*^{fl/fl} mice both had greater pulmonary bacterial burden at 21 dpi (~3.5-fold and

14-fold, respectively; Fig. 4 B). At 21 dpi, both *LysM*-Cre⁺ *Irg1*^{fl/fl} and *CD11c*-Cre⁺ *Irg1*^{fl/fl} mice had greater numbers of neutrophils in their lungs than Cre⁻ *Irg1*^{fl/fl} mice (Fig. 4, C–E), but *Mrp8*-Cre⁺ *Irg1*^{fl/fl} mice did not (Fig. 4 F). Loss of *Irg1* expression in myeloid cells (*LysM*-Cre⁺ *Irg1*^{fl/fl} mice) resulted in higher levels of cytokines and chemokines in the lungs at 21 dpi (Fig. 4 G). Loss of *Irg1* expression in alveolar macrophages and some dendritic cell subsets from *CD11c*-Cre⁺ *Irg1*^{fl/fl} mice also resulted in greater amounts of inflammatory cytokines and chemokines. In comparison, deletion of *Irg1* in neutrophils had little effect on cytokine responses. These data show that *Irg1* expression in CD11c⁺ and *LysM*⁺ cell subsets regulates neutrophil recruitment and inflammation. Although neutrophils mediate *Mtb*-induced immunopathology in *Irg1*^{-/-} mice, their cell-intrinsic expression of *Irg1* is dispensable for this process.

To gain insight into why a lack of *Irg1* expression in myeloid cells resulted in excessive accumulation of neutrophils in *Irg1*^{-/-} mice during *Mtb* infection, we compared the expression profiles of *Mtb*-infected WT and *Irg1*^{-/-} BMDMs. Within just 4 h of *Mtb* infection, the transcriptional signature in *Irg1*^{-/-} BMDMs differed markedly from WT BMDMs. Many of the genes that were up-regulated in *Irg1*^{-/-} cells after *Mtb* infection were down-regulated in WT BMDMs (Fig. 5 A). Exogenous addition of physiologically relevant doses of itaconate (0.25 mM; Michelucci et al., 2013; Lampropoulou et al., 2016) to *Mtb*-infected *Irg1*^{-/-} BMDMs switched the transcriptional signature to one similar to *Mtb*-infected WT BMDMs (Fig. 5 A). This result suggests that the effect of *Irg1* deletion on transcriptional profiles was principally a result of the loss of itaconate production. Pathway enrichment analysis indicated that a lack of *Irg1* expression in *Mtb*-infected BMDMs resulted in induction of inflammatory and chemoattractant genes downstream of NF-κB signaling, and correspondingly, addition of itaconate to *Irg1*^{-/-} BMDMs reverses this effect (Fig. 5, B and C). These data show that *Irg1* and its product itaconate function to limit inflammation during *Mtb* infection at the transcriptional level.

How does *Irg1* regulate inflammation during *Mtb* infection? *Irg1* has been reported to suppress production of TLR-triggered NF-κB-dependent cytokines, including TNF-α, through induction of the negative regulator A20 (Li et al., 2013; Jamal Uddin et al., 2016). Although an increased inflammatory response was detected in the lungs of *Irg1*^{-/-} mice at 14 dpi, we failed to detect differences in TNF-α levels compared with WT lung homogenates. Thus, in the context of *Mtb* infection *Irg1* appears to modulate inflammatory responses by dampening expression of a selected subset of NF-κB regulated genes. Analogously,

Figure 2. Irg1 modulates inflammatory responses in the lung after Mtb infection. Mice were infected with aerosolized *Mtb*-GFP. (A) Histopathology was visualized by H&E staining of lungs at 21 dpi. Images are representative of two independent experiments. Bars: 2.5 mm (1.25×); 50 μm (40×). (B) Flow cytometry plots for neutrophils as a percentage of total CD45⁺ cells in lungs before *Mtb* infection and at 10, 14, and 21 dpi. Data are representative of results from *n* = 6–15 mice depending on the time point. (C–E) Number of innate immune cell populations in lungs at 10 dpi (C; *n* = 6), 14 dpi (D; *n* = 10), and 21 dpi (E; *n* = 6–15). (F–H) Cytokine and chemokine levels in the *Mtb*-infected lungs at 10 dpi (F; *n* = 6), 14 dpi (G; *n* = 10), and 21 dpi (H; *n* = 6). (I) Acid-fast bacilli in *Mtb*-infected lungs at 21 dpi. Images are representative of two independent experiments. Bars, 10 μm. (J) Flow cytometry plots for *Mtb*-GFP⁺ neutrophils in lungs at 10, 14, and 21 dpi. SSC, side scatter. (K) The percentage of *Mtb*-GFP-positive cells in indicated cell types at 10 (*n* = 6), 14 (*n* = 8–10), and 21 (*n* = 6–15) dpi. All data are pooled from at least two independent experiments. (C–H and K) Bars indicate median values. Statistical differences were determined by Mann-Whitney test (*, *P* < 0.05; **, *P* < 0.01; ***, *P* < 0.001; ****, *P* < 0.0001; ns, not significant). Mφ, macrophages. See also Figs. S1 and S2.

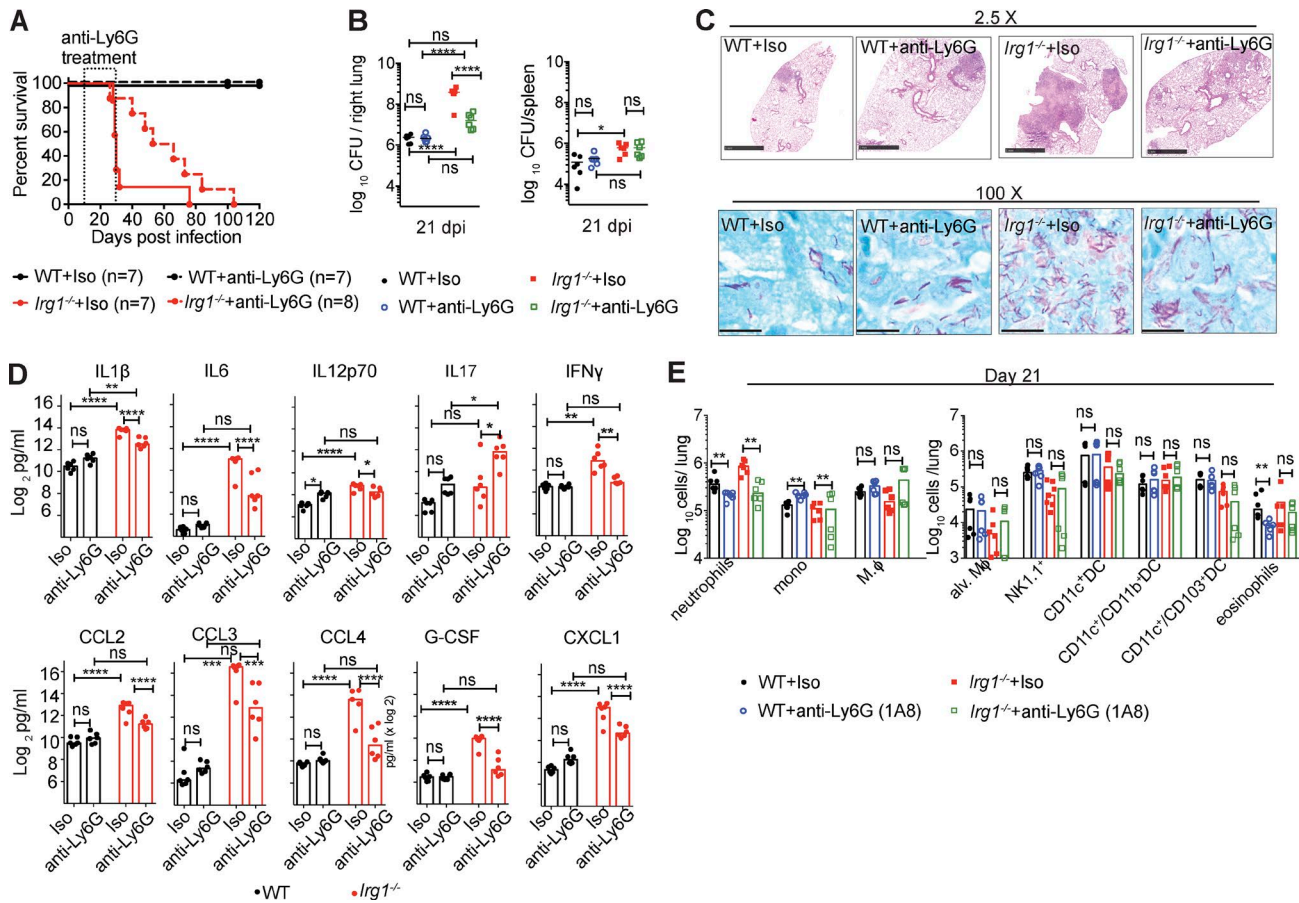


Figure 3. Depletion of neutrophils enhances survival of *Mtb*-infected *Irg1*^{-/-} mice. WT and *Irg1*^{-/-} mice were infected with aerosolized *Mtb* and treated with anti-Ly6G or isotype control antibodies as described in the Materials and methods. **(A)** Survival analysis ($n = 7-8$). **(B)** *Mtb* burden in the lung at 21 dpi ($n = 7-8$). Lines indicate median values. **(C)** Lung histopathology and acid-fast bacilli at 21 dpi were visualized with H&E (top) and acid-fast (bottom) stains. Images are representative of two independent experiments. Bars: 1 mm (top); 100 μ m (bottom). **(D)** Cytokine levels at 21 dpi ($n = 6$). **(E)** Innate immune cell populations in the lung at 21 dpi ($n = 6$). All data are pooled from two independent experiments. Statistical differences were determined via one-way ANOVA with Tukey's correction (B and D) and Mann-Whitney test (E); *, $P < 0.05$; **, $P < 0.01$; ***, $P < 0.001$; ****, $P < 0.0001$; ns, not significant). See also Fig. S2.

exogenous itaconate treatment of activated macrophages or LPS treatment of *Irg1*^{-/-} macrophages also did not affect TNF- α levels relative to their respective controls (Lampropoulou et al., 2016).

In summary, our experiments establish an essential role of Irg1 in regulating neutrophil-dependent inflammation during *Mtb* infection of the lung. We show that Irg1, likely through its ability to convert the TCA cycle intermediate cis-aconitate to itaconate, shapes the host immune responses through an immunometabolism axis to curtail *Mtb*-induced lung disease. As mouse Irg1 is ~80% identical in amino acid sequence to human IRG1 with all five predicted cis-aconitate decarboxylase domains fully conserved (Michelucci et al., 2013), the development of pharmacological agents that enhance Irg1 function or promote itaconate production might minimize pathological inflammatory responses that cause severe lung injury associated with TB disease progression.

Materials and methods

Ethics statement

All procedures involving animals were conducted following the National Institutes of Health (NIH) guidelines for housing and

care of laboratory animals and performed in accordance with institutional regulations after protocol review and approval by the Institutional Animal Care and Use Committee of the Washington University in St. Louis School of Medicine (protocol no. 20160118). Washington University is registered as a research facility with the United States Department of Agriculture and is fully accredited by the American Association of Accreditation of Laboratory Animal Care. The Animal Welfare Assurance is on file with Office for Protection from Research Risks-NIH. All animals used in these experiments were subjected to no or minimal discomfort. All mice were euthanized by CO₂ asphyxiation, which is approved by the American Veterinary Association Panel on Euthanasia.

Mice

C57BL/6N (WT) mice were either purchased from Charles River or bred in-house. No differences in survival or disease progression during *Mtb* infection were observed in *Irg1*^{+/+} littermate controls or *Irg1*^{+/+} C57BL/6N mice obtained from Charles River in three independent experiments. B6.SJL (CD45.1) mice were obtained from Jackson Laboratories. *Irg1*^{-/-} mice (embryonic stem cells obtained from KOMP [C57BL/6N background,

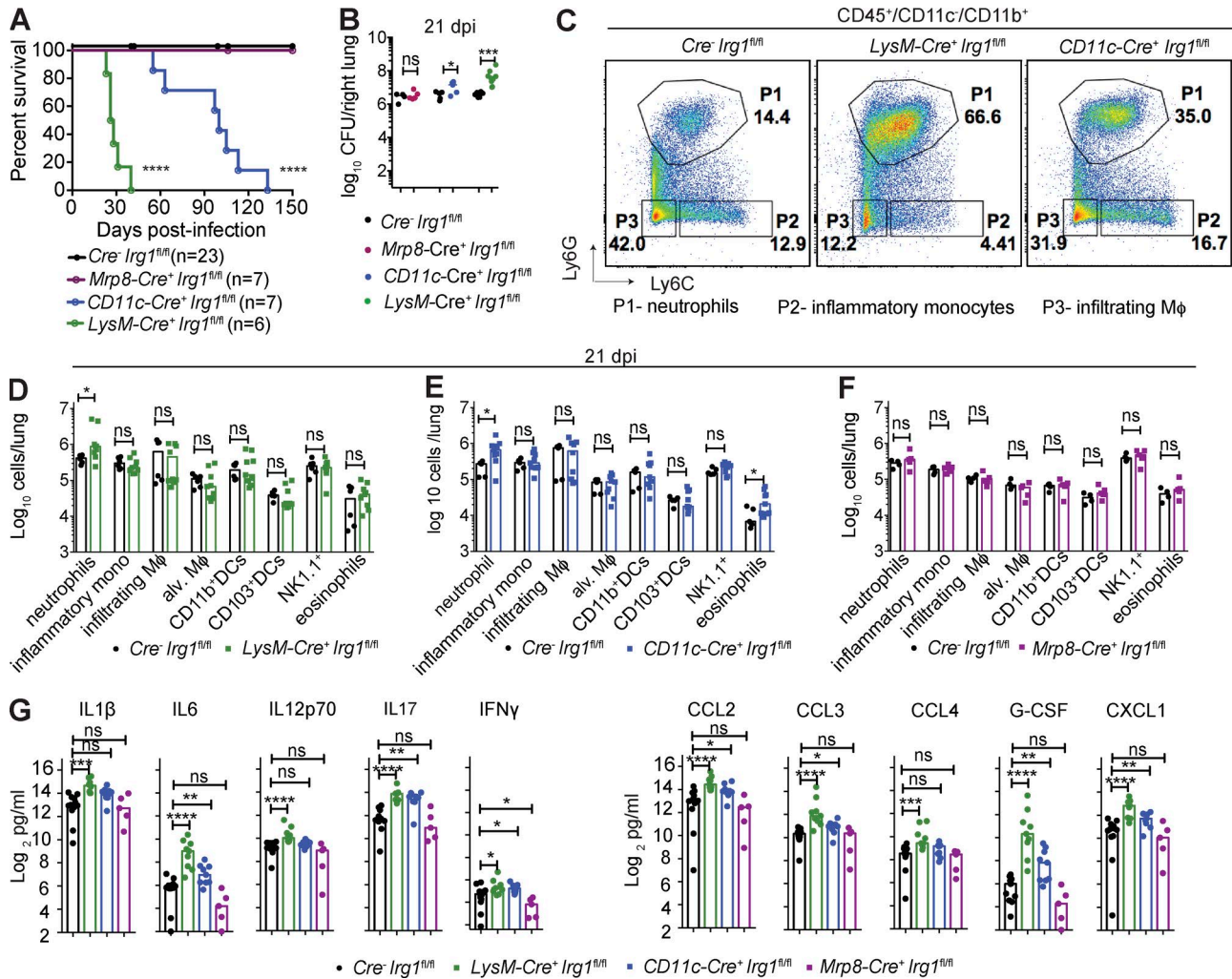


Figure 4. Loss of *Irg1* in myeloid cell subsets confers susceptibility to *Mtb*. Mice were infected with aerosolized *Mtb*. **(A)** Survival analysis of *Cre⁻ Irg1^{fl/fl}*, *Mrp8-Cre⁺ Irg1^{fl/fl}*, *CD11c-Cre⁺ Irg1^{fl/fl}*, and *LysM-Cre⁺ Irg1^{fl/fl}* mice ($n = 6-23$) after *Mtb* infection. **(B)** *Mtb* burden in lungs of *Cre⁻ Irg1^{fl/fl}* ($n = 15$), *Mrp8-Cre⁺ Irg1^{fl/fl}* ($n = 5$), *CD11c-Cre⁺ Irg1^{fl/fl}* ($n = 9$), and *LysM-Cre⁺ Irg1^{fl/fl}* ($n = 9$) mice at 21 dpi. Lines indicate median values. **(C)** Flow cytometry plots of lung neutrophils (P1), inflammatory monocytes (P2), and infiltrating macrophages (P3) as a percentage of the total CD45⁺ CD11c⁺ CD11b⁺ population in *Cre⁻ Irg1^{fl/fl}*, *LysM-Cre⁺ Irg1^{fl/fl}*, and *CD11c-Cre⁺ Irg1^{fl/fl}* mice at 21 dpi. **(D-F)** Quantitation of myeloid cells in lungs of *Cre⁻ Irg1^{fl/fl}* ($n = 6$) and *LysM-Cre⁺ Irg1^{fl/fl}* (D; $n = 9$), *Cre⁻ Irg1^{fl/fl}* ($n = 5$) and *CD11c-Cre⁺ Irg1^{fl/fl}* (E; $n = 9$), and *Cre⁻ Irg1^{fl/fl}* ($n = 4$) and *Mrp8-Cre⁺ Irg1^{fl/fl}* (F; $n = 5$) mice at 21 dpi. Mφ, macrophages. **(G)** Cytokine levels at 21 dpi ($n = 5-14$). All data are pooled from at least two independent experiments. Bars indicate median values. Statistical differences were determined via log-rank test with a Bonferroni post-hoc correction for multiple comparisons (A; ****, $P < 0.0001$) and Mann-Whitney test (B and D-G; *, $P < 0.05$; **, $P < 0.01$; ***, $P < 0.001$; ****, $P < 0.0001$; ns, not-significant). See also Fig. S3.

reporter-tagged insertion with conditional potential, MGI: 103206]) were generated at Washington University and have been described previously (Lampropoulou et al., 2016). Adult mice (6–13 wk of age) of both sexes were used, and sex was randomized between experiments. *Cre⁻ Irg1^{fl/fl}* mice were generated as described previously (Coleman et al., 2015) with two loxP sites flanking exon 4 of *Irg1*. *Irg1^{-/-}* mice were bred with *FLPe* “deleter” mice (Kanki et al., 2006) to facilitate deletion of *lacZ* and neomycin resistance cassettes between FRT sites and create *Irg1^{fl/+}* founder mice. The founder mice were backcrossed to C57BL/6/J background using speed congenic approaches (>99% purity) and then interbred to generate *Irg1^{fl/fl}* mice. These animals were crossed with *Mrp8-Cre^{-/-}*, *LysM-Cre^{-/-}* and *CD11c-Cre^{-/-}* (Jackson Laboratory) expressing mice to delete exon 4 of *Irg1* from specific subsets of myeloid cells.

Generation of bone marrow chimeric mice

Bone marrow chimeric mice were generated by irradiation (900 Gy) of WT or *Irg1^{-/-}* recipients and reconstitution with 10^7 bone marrow cells from WT or *Irg1^{-/-}* donors. 6–8 wk after bone marrow transplantation, *Irg1^{-/-}* (CD45.2) → WT (CD45.1), WT (CD45.1) → *Irg1^{-/-}* and WT (CD45.1) → WT (CD45.2), and WT (CD45.1) + *Irg1^{-/-}* (CD45.2) → WT (CD45.1) mice were bled to confirm chimerism by flow cytometry before *Mtb* infection.

Mouse infections

Mtb cultures in logarithmic growth phase ($OD_{600} = 0.5-0.8$) were washed with PBS + 0.05% Tween 80, sonicated to disperse clumps, and diluted in sterile water. Mice were exposed to 1.6×10^8 CFUs of *Mtb*, a dose chosen to deliver 100–200 CFUs of aerosolized *Mtb* per lung using an inhalation exposure system

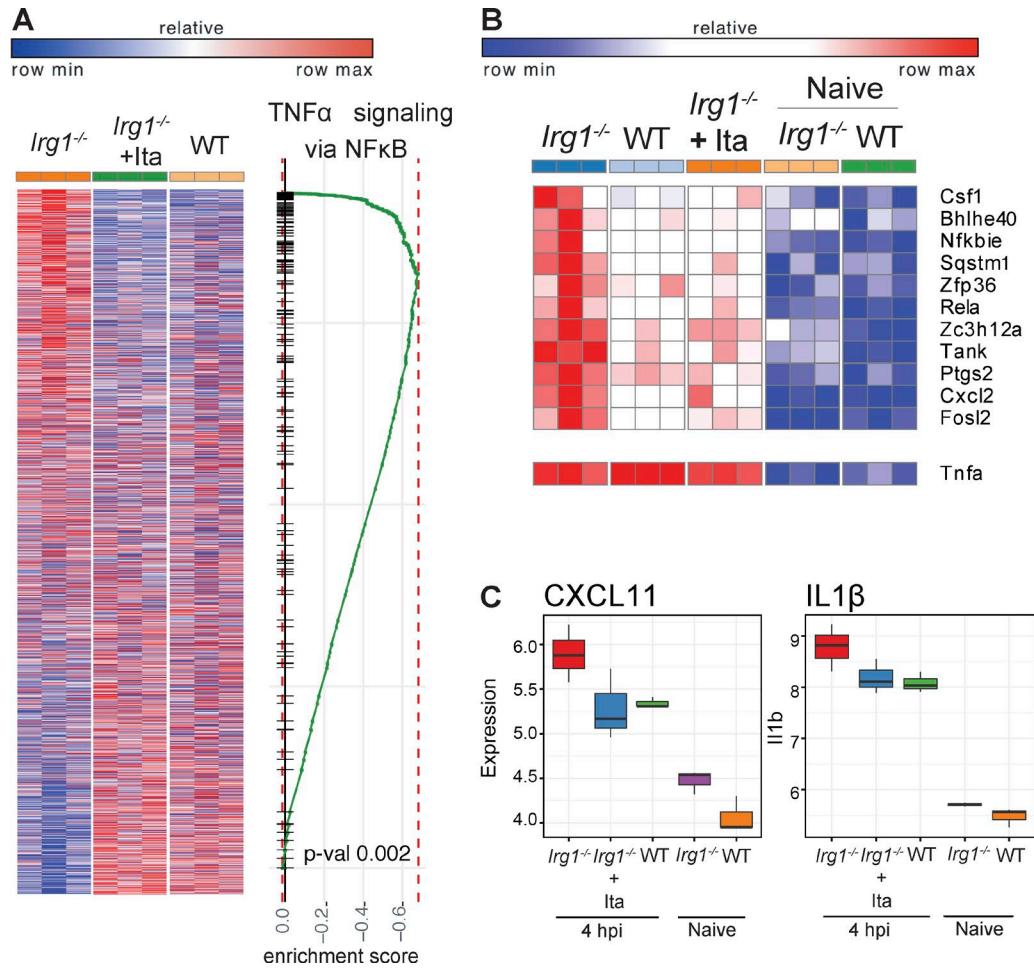


Figure 5. Irg1 alters the transcriptional signature in *Mtb*-infected BMDMs. (A–C) Transcriptomic data from WT, *Irg1*^{-/-}, and *Irg1*^{-/-} + itaconate (Ita)–treated BMDMs infected with *Mtb* and analyzed at 4 h postinfection (hpi). **(A)** Heat map comparing the transcriptional changes that occur at 4 hpi in *Irg1*^{-/-} BMDMs ± Ita and WT BMDMs (left). Genes that are up-regulated in WT BMDMs also are enriched in *Irg1*^{-/-} + itaconate BMDMs at 4 hpi. Columns and rows show conditions and genes, respectively. Genes are ranked according to significance of differential expression and direction of change. Plot shows the running score for NF-κB gene set as the analysis moves down the ranked list (right). **(B and C)** Gene set enrichment analysis comparison for genes in NF-κB signaling (B) and inflammatory chemokine CXCL11 and IL1-β (C) between WT versus *Irg1*^{-/-}, WT versus *Irg1*^{-/-} + Ita, and *Irg1*^{-/-} + Ita versus *Irg1*^{-/-} BMDMs. Error bars designate SEM.

(Glas-Col). For each infection, lungs were harvested from at least two control mice, homogenized, and plated on 7H11 agar to confirm the input CFU dose. The mean dose determined at this time point was assumed to be representative of the dose received by all other mice infected concurrently. *Mtb* burden was determined after homogenizing the superior, middle, and inferior lobes of the lung or the entire spleen and plating serial dilutions on 7H11 agar. Colonies were counted after 3 wk of incubation at 37°C in 5% CO₂.

Listeria monocytogenes (strain EGD) was stored at mid-logarithmic growth as frozen glycerol stocks. Thawed bacteria were diluted into pyrogen-free saline for intravenous injection into mice at a dose of 10⁵ bacteria/mouse in 200 μl.

Mice were infected with IAV strain A/California/04/2009 H1N1 by intranasal inoculation of 10⁵ or 10⁶ tissue culture dose. At 5 dpi viral titer was assessed from bronchoalveolar (BAL) fluid by tissue culture dose.

Neutrophil depletions

Mice were administered 200 μg of anti-Ly6G mAb (1A8; BioX-Cell) or rat IgG2a isotype control mAb (2A3; BioXCell) diluted

in sterile PBS (Hyclone) by intraperitoneal injection every 48 h, beginning at 10 dpi and ending at 20 or 34 dpi, depending on the experiment. For confirmation of depletion during survival experiments, lungs from one anti-Ly6G treated *Irg1*^{-/-} control mouse and one isotype treated *Irg1*^{-/-} control mouse were harvested from each independent experiment and analyzed by flow cytometry for reduction in CD45⁺/CD11b⁺Ly6C^{mid} cells.

Infection of BMDMs

Macrophages were obtained by culturing bone marrow cells in RPMI-1640 (Invitrogen) supplemented with 10% heat-inactivated FBS, 2 mM L-glutamine, 1% nonessential amino acids, 100 U penicillin per ml, 100 μg streptomycin per ml, and 22 ng M-CSF (Peprotech)/ml for 6 d at 37°C, 5% CO₂. Fresh media was added on day 3 of culture. After 6 d of culture, nonadherent cells were discarded. Adherent macrophages were switched into antibiotic-free media and seeded at 10⁵ cells per well and 9 × 10⁵ cells per well in tissue culture-treated 96- and 6-well plates, respectively. In some cases, macrophages were treated with physiologically relevant concentrations of 0.25 mM itaconic acid (Sigma)

for 12 h before inoculation with *Mtb* (Michelucci et al., 2013). *Mtb* was grown to midlog phase, washed with PBS, sonicated to disperse clumps, and resuspended in antibiotic-free macrophage culture media. Macrophage cultures were inoculated by adding *Mtb*-containing media at a multiplicity of infection of 1 and centrifuging for 10 min at 200 g. Cells were washed twice with PBS to remove unbound *Mtb*, fresh culture media was added, and cells were incubated at 37°C, 5% CO₂. In some cases, culture media was supplemented with 0.25 mM itaconic acid.

Bacterial cultures

Mtb strain Erdman and its derivatives were cultured at 37°C in 7H9 broth (Sigma) or on 7H11 agar (BD Difco) medium supplemented with 10% oleic acid/albumin/dextrose/catalase, 0.5% glycerol, and 0.05% Tween 80 (broth only). *Listeria monocytogenes* (strain EGD) was grown in a shaking culture in brain-heart infusion broth at 37°C to midlogarithmic growth, washed in PBS, and frozen as glycerol stocks at -80°C.

Generation of *Mtb* mutants

Mtb-GFP was generated by transforming the *Mtb* strain Erdman with a plasmid (pMV261-kan-GFP) that drives constitutive expression of GFP under the control of the *hsp60* promoter. Cultures were grown in the presence of kanamycin to ensure plasmid retention. $\Delta icl1$ *Mtb* was generated by transducing the *Mtb* strain Erdman with a phage containing homology to nucleotides 556805–557527 and 558797–559447 to replace the endogenous *icl1* gene with a hygromycin resistance cassette. Mutants were selected by culture on hygromycin-containing 7H11 agar. Individual hygromycin-resistant colonies were expanded by inoculation into hygromycin-supplemented 7H9 media. Replacement of the *icl1* gene with the hygromycin resistance cassette was confirmed by Southern blotting of genomic DNA from expanded cultures.

Viral cultures

A/California/04/2009 H1N1 influenza viral stocks were prepared as previously described (Williams et al., 2016).

BAL lavage of IAV infected mice

For analysis of BAL fluid, mice were sacrificed by Avertin overdose, followed by anterior neck dissection and cannulation of the trachea with a 22-G catheter. BAL was performed with three washes of 0.8 ml of sterile Hanks' balanced salt solution. BAL fluid was centrifuged and the cell-free supernatant was collected and stored for viral titer analysis.

Flow cytometry

Mice were perfused with sterile PBS and left lobes of lungs were digested at 37°C with 630 µg/ml collagenase D (Roche) and 75 U/ml DNase I (Sigma). All antibodies were used at a dilution of 1:200. Single cell suspensions were preincubated with Fc Block antibody (BD PharMingen) in PBS + 2% heat-inactivated FBS for 10 min at room temperature before staining. Cells were incubated with antibodies against the following markers: V500 anti-CD45.1 (clone A20), AF700 anti-CD45.2 (clone 104; eBioscience), AF700 anti-CD45 (clone 30 F-11), APC-Cy7 anti-CD11c (clone N418), PE anti-Siglec F (clone E50-2440; BD), PE-Cy7 anti-Ly6G (clone

1A8), PB or Qdot605 anti-Ly6C (clone AL-21/HK1.4; Biolegend/BD), PerCP-Cy5.5 anti-CD11b (clone M1/70), APC anti-CD103 (clone 2E7; eBioscience), PB anti-CD3 (clone 17A2), PE-Cy7, APC anti-CD4 (clone RM4-5), PE-Cy7 anti-CD8 (clone 53-6.7), anti-NK1.1 (clone PK136), and APC anti-Nos2 (clone CXNFT; all from eBioscience). Intracellular ROS were stained with MitoSOX red dye (Thermo Fisher). Absolute cell counts were determined using TruCount beads (BD). Cells were stained for 20 min at 4°C, washed, and fixed in 4% paraformaldehyde (Electron Microscopy Sciences) in PBS for 20 min at 4°C. Flow cytometry data were acquired on a cytometer (LSR Fortessa; BD Biosciences) and analyzed using FlowJo software (Tree Star). Gating strategies are depicted in Fig. S2.

Cytokine/chemokine quantification

Lungs were homogenized in 5 ml of PBS supplemented with 0.05% Tween 80. Homogenates were filtered (0.22 µm) twice and analyzed by BioPlex-Pro Mouse Cytokine 23-Plex Immunoassay (Bio-Rad).

Histology and imaging

Lung samples were fixed in 10% buffered formalin (Thermo Fisher). Gross pathology images were acquired using a Power Shot G9 camera (Canon). For detailed histological analysis, lung lobes were embedded in paraffin, sectioned, and stained with H&E (Pulmonary Morphology Core, Washington University). *Mtb* bacilli were stained with Ziehl-Neelsen stain (Pulmonary Morphology Core). Images were acquired using NanoZoomer 2.0-HT System (Hamamatsu) or an Eclipse E400 camera (Nikon).

RNA-seq

BMDMs were harvested at 4 h after *Mtb* infection, and RNA was extracted using TRIzol reagent (Invitrogen). mRNA was extracted with oligo-dT beads (Invitrogen) and cDNA synthesized using custom oligo-dT primer with a barcode and adaptor-linker sequence (CCTACACGACGCTCTTCCGATCT-XXX XXXXX-T15). Samples were pooled based on *Actb* qPCR values, RNA-DNA hybrids degraded with acid-alkali treatment and a second sequencing linker (5'-AGATCGGAAGAGCACACGTCTG-3') was ligated with T4 ligase (NEB). After SPRI bead cleanup (Agencourt AMPure XP; Beckman Coulter), the mixture was PCR-enriched (12 cycles) and SPRI-purified, yielding final strand-specific RNA-seq libraries. Libraries were sequenced on a HiSeq 2500 (Illumina) using 40 × 10 bp paired-end sequencing. Second read (read-mate) was used for sample demultiplexing. Files obtained from the sequencing center were demultiplexed with fastq-multx tool. Fastq files for each sample were aligned to mm10 genome (Release M8 Gencode; GRCm38.p4) using STAR. Each sample was evaluated according to a variety of both pre- and postalignment quality control measures with Picard tools. Aligned reads were quantified using a quant3p script (Computer Technologies Laboratory, 2016) to account for specifics of 3' sequencing: higher dependency on good 3' annotation and lower level of sequence specificity close to 3' end. Actual read counts were performed by HTSeq with enriched genome annotation and alignment with fixed multimapper flags. DESeq2 was used for analysis of differential gene expression. Preranked GSEA

analysis was used to identify pathway enrichments in hallmark and canonical pathways.

Quantification and statistical analysis

All data are from at least two independent biological experiments with multiple mice in each group. No blinding was performed during animal experiments. Statistical differences were calculated using Prism 7 (GraphPad) using log-rank Mantel-Cox tests (survival), unpaired two-tailed Mann-Whitney tests (to compare two groups with nonparametric data distribution), and one-way ANOVA with Tukey's multiple comparisons tests (to compare more than two groups with parametric data distribution). Differences with a p-value of <0.05 were defined as statistically significant.

Data and software availability

RNA-seq data are available in the Gene Expression Omnibus repository under reference series number [GSE98458](https://www.ncbi.nlm.nih.gov/geo/query/acc.cgi?acc=GSE98458).

Online supplemental materials

Further details including generation of *Mtb* mutants, protocols for bacterial cultures, viral cultures, BAL lavage, flow cytometry, chemokine/cytokine quantification, histology, imaging, RNA-seq, quantification, and statistical analysis can be found in the online supplemental methods. Fig. S1 shows that *Irg1*^{-/-} mice are susceptible to Δ *Icl1* *Mtb*, and infection of WT-*Mtb* or *Mtb*-GFP in WT and *Irg1*^{-/-} mice and BMDM. Fig. S2 defines cellular infiltrates in the lungs of WT and *Irg1*^{-/-} mice after *Mtb* infection and depletion of neutrophils in the lung. Fig. S3 shows that radio-sensitive hematopoietic cells promote Irg1-mediated responses against *Mtb* and assessment of *Irg1* exon 4 deletion in conditional gene-targeted mice.

Acknowledgments

National Institutes of Health (NIH) grants R01 AI04972 (to M.S. Diamond), R01 AI118938 (to A.C.M. Boon), R01 AI125618 (to M.N. Artyomov), a Beckman Young Investigator Award from the Arnold and Mabel Beckman Foundation (to C.L. Stallings), a Burroughs Wellcome Fund Investigator Award (to C.L. Stallings), a Career Award for Medical Scientists from the Burroughs Wellcome Fund (to B.T. Edelson), and the NIH Shared Instrumentation Grant (S10 RR027552) supported this study. The Deutsche Forschungsgemeinschaft supported S. Nair. The National Science Foundation Graduate Research Fellowship Program (DGE-1143954) supported J.P. Huynh and A. Gounder. The government of the Russian Federation, grant 074-U01, supported E. Esaulova. The authors declare no competing financial interests.

Author contributions: S. Nair, J.P. Huynh, C.L. Stallings, and M.S. Diamond conceived and designed the study. S. Nair and J.P. Huynh contributed equally and performed many of the in vivo infection experiments with *Mtb*, histology, immunological experiments, flow cytometry, and data analysis. V. Lampropoulou worked with S. Nair and J.P. Huynh in setting up in vitro infections of neutrophils. E. Loginicheva, E. Esaulova, V. Lampropoulou, and M.N. Artyomov performed the RNA-seq analysis. S. Nair and M.S. Diamond are responsible for the breeding and

genotyping of the *Irg1*^{-/-} and *Irg1*^{fl/fl} mouse colonies. A.P. Gounder and A.C.M. Boon designed and performed IAV infection experiments, and S. Nair analyzed the data. E.A. Schwarzkopf and T.R. Bradstreet performed *Listeria monocytogenes* infections, and B.T. Edelson performed the analysis. S. Nair, J.P. Huynh, M.N. Artyomov, M.S. Diamond, and C.L. Stallings contributed to study design. S. Nair and J.P. Huynh wrote the first draft of the manuscript, which was edited initially by M.S. Diamond and C.L. Stallings, and subsequently by V. Lampropoulou, M.N. Artyomov, B.T. Edelson., A.C.M. Boon, and A.P. Gounder.

Submitted: 19 January 2018

Revised: 1 February 2018

Accepted: 7 February 2018

References

- Bloch, H., and W. Segal. 1956. Biochemical differentiation of *Mycobacterium tuberculosis* grown in vivo and in vitro. *J. Bacteriol.* 72:132-141.
- Coleman, J.L., K. Brennan, T. Ngo, P. Balaji, R.M. Graham, and N.J. Smith. 2015. Rapid Knockout and Reporter Mouse Line Generation and Breeding Colony Establishment Using EUCOMM Conditional-Ready Embryonic Stem Cells: A Case Study. *Front. Endocrinol. (Lausanne)*. 6:105.
- Computer Technologies Laboratory. 2016. quant3p. A set of scripts to 3' RNA-seq quantification. Available at: <https://github.com/ctlab/quant3p> (Accessed February 27, 2018).
- Cooper, A.M., D.K. Dalton, T.A. Stewart, J.P. Griffin, D.G. Russell, and I.M. Orme. 1993. Disseminated tuberculosis in interferon gamma gene-disrupted mice. *J. Exp. Med.* 178:2243-2247. <https://doi.org/10.1084/jem.178.6.2243>
- Degrandi, D., R. Hoffmann, C. Beuter-Gunia, and K. Pfeffer. 2009. The proinflammatory cytokine-induced IRG1 protein associates with mitochondria. *J. Interferon Cytokine Res.* 29:55-68. <https://doi.org/10.1089/jir.2008.0013>
- Dunn, M.F., J.A. Ramírez-Trujillo, and I. Hernández-Lucas. 2009. Major roles of isocitrate lyase and malate synthase in bacterial and fungal pathogenesis. *Microbiology*. 155:3166-3175. <https://doi.org/10.1099/mic.0.030858-0>
- Flynn, J.L., J. Chan, K.J. Triebold, D.K. Dalton, T.A. Stewart, and B.R. Bloom. 1993. An essential role for interferon gamma in resistance to *Mycobacterium tuberculosis* infection. *J. Exp. Med.* 178:2249-2254. <https://doi.org/10.1084/jem.178.6.2249>
- Hall, C.J., R.H. Boyle, J.W. Astin, M.V. Flores, S.H. Oehlers, L.E. Sanderson, F. Ellett, G.J. Lieschke, K.E. Crosier, and P.S. Crosier. 2013. Immunoresponsive gene 1 augments bactericidal activity of macrophage-lineage cells by regulating β -oxidation-dependent mitochondrial ROS production. *Cell Metab.* 18:265-278. <https://doi.org/10.1016/j.cmet.2013.06.018>
- Höner Zu Bentrup, K., A. Miczak, D.L. Swenson, and D.G. Russell. 1999. Characterization of activity and expression of isocitrate lyase in *Mycobacterium avium* and *Mycobacterium tuberculosis*. *J. Bacteriol.* 181:7161-7167.
- Jamal Uddin, M., Y. Joe, S.K. Kim, S. Oh Jeong, S.W. Ryter, H.O. Pae, and H.T. Chung. 2016. IRG1 induced by heme oxygenase-1/carbon monoxide inhibits LPS-mediated sepsis and pro-inflammatory cytokine production. *Cell. Mol. Immunol.* 13:170-179. <https://doi.org/10.1038/cmi.2015.02>
- Kanki, H., H. Suzuki, and S. Itohara. 2006. High-efficiency CAG-FLPe deleter mice in C57BL/6J background. *Exp. Anim.* 55:137-141. <https://doi.org/10.1538/expanim.55.137>
- Kimmey, J.M., J.P. Huynh, L.A. Weiss, S. Park, A. Kambal, J. Debnath, H.W. Virgin, and C.L. Stallings. 2015. Unique role for ATG5 in neutrophil-mediated immunopathology during *M. tuberculosis* infection. *Nature*. 528:565-569. <https://doi.org/10.1038/nature16451>
- Lampropoulou, V., A. Sergushichev, M. Bambouskova, S. Nair, E.E. Vincent, E. Loginicheva, L. Cervantes-Barragan, X. Ma, S.C. Huang, T. Griss, et al. 2016. Itaconate Links Inhibition of Succinate Dehydrogenase with Macrophage Metabolic Remodeling and Regulation of Inflammation. *Cell Metab.* 24:158-166. <https://doi.org/10.1016/j.cmet.2016.06.004>
- Li, Y., P. Zhang, C. Wang, C. Han, J. Meng, X. Liu, S. Xu, N. Li, Q. Wang, X. Shi, and X. Cao. 2013. Immune responsive gene 1 (IRG1) promotes endotoxin tolerance by increasing A20 expression in macrophages through

- reactive oxygen species. *J. Biol. Chem.* 288:16225–16234. <https://doi.org/10.1074/jbc.M113.454538>
- McFadden, B.A., and S. Purohit. 1977. Itaconate, an isocitrate lyase-directed inhibitor in *Pseudomonas indigofera*. *J. Bacteriol.* 131:136–144.
- McKinney, J.D., K. Höner zu Bentrup, E.J. Muñoz-Elías, A. Miczak, B. Chen, W.T. Chan, D. Swenson, J.C. Sacchettini, W.R. Jacobs Jr., and D.G. Russell. 2000. Persistence of *Mycobacterium tuberculosis* in macrophages and mice requires the glyoxylate shunt enzyme isocitrate lyase. *Nature.* 406:735–738. <https://doi.org/10.1038/35021074>
- Michelucci, A., T. Cordes, J. Ghelfi, A. Pailot, N. Reiling, O. Goldmann, T. Binz, A. Wegner, A. Tallam, A. Rausell, et al. 2013. Immune-responsive gene 1 protein links metabolism to immunity by catalyzing itaconic acid production. *Proc. Natl. Acad. Sci. USA.* 110:7820–7825. <https://doi.org/10.1073/pnas.1218599110>
- Muñoz-Elías, E.J., and J.D. McKinney. 2005. *Mycobacterium tuberculosis* isocitrate lyases 1 and 2 are jointly required for in vivo growth and virulence. *Nat. Med.* 11:638–644. <https://doi.org/10.1038/nm1252>
- Muñoz-Elías, E.J., A.M. Upton, J. Cherian, and J.D. McKinney. 2006. Role of the methylcitrate cycle in *Mycobacterium tuberculosis* metabolism, intracellular growth, and virulence. *Mol. Microbiol.* 60:1109–1122. <https://doi.org/10.1111/j.1365-2958.2006.05155.x>
- Nandi, B., and S.M. Behar. 2011. Regulation of neutrophils by interferon- γ limits lung inflammation during tuberculosis infection. *J. Exp. Med.* 208:2251–2262. <https://doi.org/10.1084/jem.20110919>
- Savvi, S., D.F. Warner, B.D. Kana, J.D. McKinney, V. Mizrahi, and S.S. Dawes. 2008. Functional characterization of a vitamin B12-dependent methylmalonyl pathway in *Mycobacterium tuberculosis*: implications for propionate metabolism during growth on fatty acids. *J. Bacteriol.* 190:3886–3895. <https://doi.org/10.1128/JB.01767-07>
- Williams, G.D., A.K. Pinto, B. Doll, and A.C. Boon. 2016. A North American H7N3 Influenza Virus Supports Reassortment with 2009 Pandemic H1N1 and Induces Disease in Mice without Prior Adaptation. *J. Virol.* 90:4796–4806. <https://doi.org/10.1128/JVI.02761-15>
- World Health Organization. 2016. Global tuberculosis report. <http://apps.who.int/medicinedocs/documents/s23098en/s23098en.pdf>